Clay Minerals (2021), **56**, 269–283
doi:10.1180/clm.2022.7

CAMBRIDGE UNIVERSITY PRESS

Article

Enhanced alumina extraction from kaolin by thermochemical activation using charcoal

Amr B. ElDeeb[1,2*], Vyacheslav N. Brichkin[1], Martin Bertau[3], Mahmoud E. Awad[4,5] and Yulia A. Savinova[6]

[1]Metallurgy Department, Saint Petersburg Mining University, Saint Petersburg, Russia; [2]Mining and Petroleum Department, Faculty of Engineering, Al-Azhar University, Nasr City, 11884, Cairo, Egypt; [3]Institute of Chemical Technology, Freiberg University of Mining and Technology, Freiberg, Germany; [4]Department of Geology, Faculty of Science, Al-Azhar University, Nasr City, 11884, Cairo, Egypt; [5]Andalusian Institute of Earth Sciences (IACT-CSIC), University of Granada, Spain and [6]Pyrometallurgy Laboratory, Gipronickel Institute, Saint Petersburg, Russia

Abstract

The present work aims to increase the alumina percentage recovery (APR) extracted from kaolin *via* the addition of 0.5–4.0 wt.% charcoal as a thermochemical fluxing agent in the lime-sintering process at 1260–1360°C. The transformation, microstructural and microtextural changes and self-disintegration performance were characterized using thermogravimetric analysis and differential scanning calorimetry, X-ray diffraction/X-ray fluorescence, scanning electron microscopy coupled with energy-dispersive spectroscopy and laser diffraction particle-size distribution analysis. The optimum enhancement of APR, from 77.7% to 87.40%, was obtained by sintering at 1360°C with the addition of 1.5% charcoal. With further increase of the charcoal content to 4%, the APR reduced to 75.6%. Combustion of ≤1.5% charcoal provided additional heat that amorphized the crystalline calcium aluminate into highly leachable amorphous phases with improved self-disintegration efficiency. Sintering at temperatures of >1360°C or with charcoal contents >4% led to mullite crystallization and decreased alumina leachability, thereby reducing the APR. Charcoal is a cost-effective and energy-efficient activator to increase the APR extracted from kaolin.

Keywords: alumina production, charcoal-based activation, kaolin, lime-sintering process, pyro-hydrometallurgy, self-disintegration process

(Received 5 August 2021; revised 14 January 2022; Accepted Manuscript online: 31 January 2022; Editor: George E. Christidis)

In recent years, large global kaolin resources have attracted considerable attention as an alternative raw material to substitute for exhausted bauxite deposits (i.e. the principal aluminium ore worldwide). Kaolinite, which contains ~39% Al_2O_3 (Murray, 2006), has been targeted for alumina production because of its abundance in the Earth's crust and because of its cost-effectiveness for recovering Al compared to other Al-bearing minerals (e.g. corundum, spinel, muscovite and alunite with respective Al_2O_3 contents of ~100%, 72%, 38% and 37%; Mikhailova *et al.*, 2007; Biagioni & Pasero, 2014; Vdovets, 2020; Li *et al.*, 2021). In addition, kaolinite has the greatest Al_2O_3 content among all of the more abundant clay minerals (e.g. montmorillonite and illite with Al_2O_3 contents of ~19% and 17%, respectively; Battaglia, 2004; Uddin, 2008). Moreover, kaolinite exhibits an intrinsically lower hardness (leading to cost-effective and energy-efficient grindability for producing ultrafine powders dominated by <2 μm size fractions) and a relatively low temperature of thermal decomposition (457–711°C) compared to non-clay Al-silicates (orthoclase, plagioclase, nepheline, leucite, kyanite and pyrope-garnet; Scorzelli *et al.*, 2008; Aldabsheh *et al.*, 2015; ElDeeb & Brichkin, 2018; Erdemoğlu *et al.*, 2018; Nzeukou Nzeugang *et al.*, 2018; Brichkin *et al.*, 2019; ElDeeb *et al.*, 2019; Pak *et al.*, 2019; Tantawy & Alomari, 2019; Sule & Sigalas, 2020; Küster *et al.*, 2021).

Generally, two processes have been proposed for Al_2O_3 extraction from clays and low-grade aluminium ores: the first is an acid process that uses sulfuric acid, hydrochloric acid or nitric acid to selectively dissolve the Al_2O_3, usually following calcination of the clay (Al-Zahrani & Abdul-Majid, 2009; Ajemba & Onukwuli, 2012; Olaremu, 2015; Toama *et al.*, 2018); the second is an alkali process that uses water or a dilute alkali to selectively dissolve the Al_2O_3 from a sintered mixture of lime and clay or lime, soda and clay (Al-Ajeel *et al.*, 2014; Guo *et al.*, 2014; Li *et al.*, 2014b; Zhang *et al.*, 2015a, 2015b). The acidic leaching methods have disadvantages including difficult leaching conditions (i.e. leaching time, temperature and acid concentration, especially in low-grade aluminium ores) when compared with the alkaline leaching methods, in addition to the corrosion problems encountered by the leaching equipment due to acidic leaching. In addition, the amount of Al_2O_3 produced by acidic leaching is less than that produced by alkaline leaching due to the lower selectivity of acidic leaching agents. Therefore, complex purification techniques have been proposed to overcome the disadvantages of the acidic leaching process (Olaremu, 2015; Valeev *et al.*, 2016).

Lime sintering has been considered to be the most appropriate and promising sintering method for Al_2O_3 extraction from kaolin among the combined pyro-hydrometallurgical processes, including the Bayer, soda-lime-sintering and lime-sintering methods. In the lime-sintering process, the kaolin fraction is proportionally mixed with limestone and the charge is then sintered at the

*E-mail: engbasuony87@yahoo.com

Cite this article: ElDeeb AB, Brichkin VN, Bertau M, Awad ME, Savinova YA (2021). Enhanced alumina extraction from kaolin by thermochemical activation using charcoal. *Clay Minerals* **56**, 269–283. https://doi.org/10.1180/clm.2022.7

optimum temperature (1360°C). During the sintering stage, the calcite component is decomposed completely into lime while the kaolinite is dehydroxylated to metakaolinite. These very chemically reactive phases form the leachable calcium aluminate compounds ($12CaO.7Al_2O_3$) and the dicalcium silicate compound ($2CaO.SiO_2$; C_2S), a non-leachable residual impurity. The Al_2O_3 content is then extracted efficiently from these calcium aluminate compounds *via* a hydrometallurgical leaching process using sodium carbonate solutions followed by washing with hot distilled water and by filtration, which yields a white sludge. The white sludge has the appropriate chemical and physical composition to make it suitable for the production of Portland cement (Chou & Burnet, 1981; Ptáček *et al.*, 2013; Al-Ajeel *et al.*, 2014; Zhang *et al.*, 2015b; Sizyakov, 2016; Tian *et al.*, 2016b; Stange *et al.*, 2017; Azof *et al.*, 2019; ElDeeb *et al.*, 2019, 2020a).

The lime-sintering process is the most cost-effective, time-efficient and energy-efficient method for alumina extraction from kaolin at 1360°C when compared with the other pyro-hydrometallurgical methods (i.e. the Bayer and the soda-lime-sintering methods; ElDeeb *et al.*, 2019, 2020a). The advantages of the lime-sintering process result from the transformation of β-C_2S into its γ-polymorph counterpart during the cooling stage. The resulting sinter self-decomposes into an ultrafine powder with a larger specific surface area that does not require pre-leach grinding and shows good leaching performance with minimal reagent consumption (Al-Ajeel *et al.*, 2014; ElDeeb *et al.*, 2019, 2020a; Pak *et al.*, 2019). Moreover, the resulting white sludge usually has a low Na_2O content when compared with the resultant sludges produced by the soda-lime-sintering and Bayer methods and does not require intensive washing (Smith, 2009; Kaußen & Friedrich, 2018). The addition of soda ash (Na_2CO_3) in the case of the soda-lime-sintering method produces the sodium aluminate phase ($Na_2O.Al_2O_3$) which prevents self-decomposition and hence represents an additional cost in the pre-leach grinding process (Bai *et al.*, 2010; Guo *et al.*, 2014; Tian *et al.*, 2016a; Yan *et al.*, 2017; Toama *et al.*, 2018). From an environmental viewpoint, the carbon dioxide (CO_2) emissions from the sintering process are normally exploited as a by-product in the carbonization process for alumina precipitation from the alumina-rich solution (Gao *et al.*, 2020).

Amorphization of the crystalline Al-bearing silicate phases into easily leachable amorphous phases is the most important process that controls Al_2O_3 extractability and recovery from the targeted non-bauxitic raw materials. It is mainly based on the ore grade and impurities in addition to the mineralogical and chemical composition and structural characteristics of the ore. The amorphization can be achieved *via* one or more synergetic combinations of the four common technological activation and treatment processes (which are mainly energy-efficient and cost-effective), including the thermal, mechanical, mechanochemical and thermochemical methods (Gasparini *et al.*, 2013; Cao *et al.*, 2016). The treatment of kaolins is achieved *via* thermal activation during the sintering process at a controlled temperature. Dehydroxylation is the main mechanism in thermal activation, which results in the complete decomposition of the kaolinite structure into a quasi-amorphous material that is easily dissolved in dilute acidic and alkaline solutions, thereby increasing the leaching efficiency and Al_2O_3 recovery (Li *et al.*, 2014a; Xu *et al.*, 2015; Zhou *et al.*, 2015; Birinci *et al.*, 2017; D'Elia *et al.*, 2018; Erdemoğlu *et al.*, 2018; Yuan *et al.*, 2018). Mechanical treatment with high-energy ball milling increases the specific surface area and structural disorder, decreases the apparent density and leads to amorphization of the kaolinite crystal structure. Hence, partial mechanical treatment also reduces the temperature of decomposition by increasing the structural disorder, thereby increasing the rate of phase transformation reactions during the sintering processes and increasing of leaching selectivity and efficiency (Tang *et al.*, 2010; Erdemoğlu & Baláž, 2012; Allegretta *et al.*, 2016; Guo *et al.*, 2016).

Recently, ElDeeb *et al.* (2019, 2020a) applied the self-disintegration process by sintering kaolin with lime (lime-sintering process) at 1360°C, which is cost- and energy-effective and time-efficient, and therefore it is not necessary to grind the resulting sinter before leaching. The addition of fluxing agents such as charcoal to the kaolin-limestone mixtures in the sintering process would increase cost-effectiveness and energy-efficiency by reducing the temperature limit of the phase transformation (i.e. β-C_2S to γ-phases). Moreover, the addition of charcoal would significantly improve the surface properties of the self-disintegrated sinter powders and particles and hence would increase leaching and maximize the alumina percentage recovery (APR; Qiu *et al.*, 2004; Sizyakov *et al.*, 2013a, 2013b; Dubovikov *et al.*, 2018; Sizyakov & Brichkin, 2018; Li *et al.*, 2019). Previous work showed that other compounds such as MgO, Al_2O_3, Fe_2O_3, BaO, B_2O_3, Na_2O, K_2O, P_2O_5, MnO_2 and Cr_2O_3, present either as chemical impurities or as fluxing additives to kaolin, were unfavourable because they stabilized the β-C_2S phase and hence prevented self-disintegration (Wang *et al.*, 2011; Yu *et al.*, 2012, 2014, 2019; Guo *et al.*, 2014; Yan *et al.*, 2017; Bazhirov *et al.*, 2020).

The use of Na_2O and FeO as fluxing agents to enhance Al_2O_3 extraction from the sintered kaolin and calcium carbonate produced solid solutions rich in $C_{12}A_7$ but inhibited the transformation of β-$2CaO.SiO_2$ to γ-$2CaO.SiO_2$ and hence the self-disintegration process (Wang *et al.*, 2011, 2017; Yu *et al.*, 2012, 2014). Yu *et al.* (2019) indicated that the self-disintegration of the sinters deteriorated with increasing phosphorous (P) content. In addition, the leaching rate of Al_2O_3 from the calcium aluminate sinters (and hence the APR) decreased with increasing P content by >0.5% as a result of the reduced self-disintegration. Therefore, the addition of 1.5–4.0 wt.% charcoal was considered to be the ideal amount of this fluxing agent because it initiated the self-disintegration process at a lower sintering temperature (1260°C) and increased cost-effectiveness as the resulting sinters did not require any pre-leach grinding. The chemical purity of the initial feed components had a significant effect on the self-disintegration process. As the chemical impurities were traces in the bulk composition of the precursor raw materials (kaolin and limestone; ElDeeb *et al.*, 2020a), they did not have any undesirable effects on the efficiency of the self-disintegration process.

The functionality of charcoal as a fluxing agent for the thermochemical activation of the limestone–kaolin mixture to increase the recovery of the extracted alumina has yet to be studied. The addition of charcoal for this purpose is considered cost-effective, energy-effective and time-efficient. Therefore, the present study aims to examine, for the first time, the effects of thermochemical activation using charcoal as a fluxing additive on the microstructural changes, phase transformations, self-disintegration, leaching and hence Al_2O_3 recovery from the sintered limestone–kaolin mixture in Al_2O_3 extraction using the lime-sintering process.

https://doi.org/10.1180/clm.2022.7 Published online by Cambridge University Press

Materials and methods

Raw materials

A high-grade white kaolin raw material collected from the Irkutsk mining site (Ivanov *et al.*, 2019) and a white limestone with some faint reddish tints obtained from the Pikalevo region, Russia (Sizyakov *et al.*, 2016) were used in the present study. The chemical and mineralogical compositions and the thermal characteristics of the raw kaolin and limestone samples were studied in detail in our previous works (ElDeeb *et al.*, 2019, 2020a). The kaolin is composed of 31.9% Al_2O_3, 52.2% SiO_2, 1.4% Fe_2O_3, 0.6% TiO_2, 0.15% Na_2O and 0.15% K_2O corresponding to 81% kaolinite, 17% quartz and 2% Fe-Ti minerals (Awad *et al.*, 2018b). The limestone is composed of 53.3% CaO (i.e. 95% calcite). A high-grade commercial charcoal composed of 86% fixed carbon and 8% volatiles and ash was purchased from Kyiv Company for Reagents (RIAP), Russia. The sodium carbonate (Na_2CO_3 of analytical grade) used in the leaching process was purchased from Vekton Company, Russia.

Sample preparation and sintering

The kaolin and limestone samples were crushed, pulverized and sieved to <74 μm. The limestone-kaolin mixture samples were prepared based on stoichiometric molar ratios using the bulk oxide contents: $CaO/SiO_2 = 2.0$, $CaO/Al_2O_3 = 1.8$ and $CaO/Fe_2O_3 = 1.0$. The optimum proportional masses of the mixed kaolin and limestone powder fractions were 100.0 and 265.8 g, respectively, because these proportions yielded efficient leaching of aluminate phases and the maximum APR in our previous study (ElDeeb *et al.*, 2020a).

To study the effects of the addition of charcoal, seven batch samples of kaolin-limestone-charcoal powder mixtures were formulated with charcoal contents of 0, 0.5, 1.0, 1.5, 2.0, 3.0 and 4.0 wt.%. The formulated components of each sample were mixed thoroughly using a reversing drum mixer in which the entire drum rotated around its axis at a rotation speed of 150 rpm. The materials were charged and discharged through a charge chute at one end of the drum with the addition of steel balls, which aided in the mixing process, and then the drum was rotated at the predetermined speed for 4 h. Then the mixtures were moulded into cylindrical briquettes (30 mm in diameter and 30 mm in height) using a Laptuls hydraulic press at 5 MPa pressure to ensure homogeneous sintering of the final resulting sinters (ElDeeb *et al.*, 2019).

To determine the optimum effective charcoal content in terms of the sintering and leaching characteristics, the seven formulated briquettes were sintered in a closed system in a PVK-1.6-5 high-temperature chamber furnace (TEPLOPRIBOR) with a heating rate of 10°C min^{-1} up to the highest temperature of 1360°C. The largest amount of charcoal added was 4% because the addition of more than 4% had a negative effect on the APR. This may be attributed to the release of excessive heat for large charcoal contents, which leads to the formation of an undesirable stable mullite phase ($Al_2O_3.SiO_2$), from which Al_2O_3 is only extracted with difficulty. To examine the effects of the optimum charcoal content (i.e. 1.5%, which produced the greatest APR) at various sintering temperatures, six replicated briquettes with 1.5 wt.% charcoal contents were heated to various final sintering temperatures of 1260°C, 1280°C, 1300°C, 1320°C, 1340°C and 1360°C.

For all of the sintered briquettes, the soaking time was 1 h. Subsequently, the sinters were annealed in the furnace by cooling them to room temperature at a rate of 10°C min^{-1} to achieve the self-disintegration process (Pontikes *et al.*, 2010; ElDeeb *et al.*, 2020a). Chromatic changes, which were considered as a proxy, were determined on the surfaces of all of the briquettes to monitor sintering homogeneity.

Alumina-leaching process

All of the sintered briquettes were subjected to leaching with sodium carbonate solutions. The leaching process takes place according to the dissociation reaction mechanisms shown in Equations 1 and 2.

$$12CaO \cdot 7Al_2O_3 + 12Na_2CO_3 + 5H_2O \rightarrow 14NaAlO_2 + 12CaCO_3 + 10NaOH \quad (1)$$

$$CaO \cdot Al_2O_3 + Na_2CO_3 \rightarrow 2NaAlO_2 + CaCO_3 \quad (2)$$

The leaching process was carried out in parallel mode in a HEL Auto-Mate II reactor system equipped with a mechanical stirrer. The liquid solution in the reactor was maintained at atmospheric pressure conditions by connecting the reflux condensers to the reaction volume to return the condensate. Stirring was carried out using a stirrer with a magnetic drive in the working zone of each reactor. The speed of rotation of the mixer varied from 250 to 1500 rpm. Temperature control was achieved using sensors installed in the reaction medium and in the jacket of each reactor. To maintain the desired temperature, each thermostatic cell was equipped with an independent heating element, and cooling was achieved by supplying a coolant *via* circulating thermostat. The operating temperature range of the system was 20–160°C ± 0.1°C. Following the procedure described by ElDeeb *et al.* (2020a), each self-disintegrated sinter powder was stirred for 15 min in a fresh Na_2CO_3 solution with a concentration of 120 g L^{-1} (1:5 solid:liquid ratio) at 70°C and 600 rpm, which yielded a suspended slurry. The pulp was filtered with a vacuum pump, producing a sludge that was washed with hot distilled water and dried at 110°C. Based on the changes in the chemical compositions of the precursor sinters and their resulting sludges, as observed from the X-ray fluorescence (XRF) data, the APR was calculated according to Equation 3:

$$Al_2O_{3\ extracted} = (Al_2O_{3\ sintered} - Al_2O_{3\ sludge})/Al_2O_{3\ sintered} \quad (3)$$

Three replicate measurements/experiments were conducted for each condition and the average was taken with the calculated standard deviation (SD) of ±2% (Tables 1 & 2).

Characterization methods

To investigate the thermal changes during the decomposition of the kaolin-limestone and kaolin-limestone-charcoal mixtures, thermogravimetric analysis (TGA) and differential scanning calorimetry (DSC) were performed with a simultaneous DSC-TGA instrument (SDT Q600, TA Instruments, USA) in the range 25–1300°C, with a heating rate of 20°C min^{-1}, under vacuum and using a platinum crucible. The mineralogical changes in the sinters and sludges were detected using X-ray diffraction (XRD) with a Bruker D8 focus X-ray diffractometer, with Cu-*Kα* radiation (40 kV, 30 mA, λ = 1.5406 Å) in the range 10–60°2θ, using a scanning step of 0.008°2θ and a counting

https://doi.org/10.1180/clm.2022.7 Published online by Cambridge University Press

Table 1. Effects of the variable amounts of charcoal added on the APR of the kaolin-limestone-charcoal mixtures sintered at 1360°C.

Charcoal added (%)	APR (%)				Conditions
	APR_1	APR_2	APR_3	$APR_{Average}$	
0	77.8	77.2	78.1	77.7	Roasting temperature = 1360°C
0.5	82.8	82.0	84.5	83.1	Leaching time = 15 min
1.0	84.1	86.0	83.1	84.4	Na_2CO_3 solution = 120 g L^{-1}
1.5	87.5	85.9	88.8	87.4	Solid:liquid ratio = 1:5
2.0	79.2	81.0	78.1	79.4	Leaching temperature = 70°C
3.0	75.6	76.9	75.7	76.0	Stirring speed = 600 rpm
4.0	74.6	75.8	76.5	75.6	

Table 2. Effects of the variable sintering temperatures on the APR with the addition of 1.5% charcoal.

Sintering temperature (°C)	APR (%)				Conditions
	APR_1	APR_2	APR_3	$APR_{Average}$	
1260	44.3	45.0	43.9	44.4	Charcoal amount = 1.5%
1280	48.5	47.9	49.1	48.5	Leaching time = 15 min
1300	68.2	69.1	67.8	68.4	Na_2CO_3 solution = 120 g L^{-1}
1320	74.5	75.8	76.1	75.5	Solid:liquid ratio = 1:5
1340	78.4	78.3	79.0	78.6	Leaching temperature = 70°C
1360	87.5	85.9	88.8	87.4	Stirring speed = 600 rpm

time of 10 s $step^{-1}$. The chemical changes in the sinters and sludges were determined using XRF with a sequential XRF spectrometer (XRF-1800, 40 kV, 90 mA, Re anode, Shimadzu, USA). Microcompositional and microstructural changes in the transformed phases were investigated using scanning electron microscopy (SEM; Tescan TS 5130MM) with a microscope equipped with an energy-dispersive X-ray (EDX) detector (active crystal area = 50 mm^2; Oxford Instruments, UK) and an INCA Energy microanalysis system and YAG crystal as the back-scattered electron detector. Particle-size analyses were performed on the powders of the sinters and sludges using laser diffraction with a domestic Microsizer 201C analyser (InTechSA Ltd, Russia) in the size range of 0.2–600 μm.

Results and discussion

Effects of charcoal addition on thermal behaviour

Based on the TGA/DSC curves of the kaolin-limestone mixture (Fig. 1a), as well as on their previously examined thermal characteristics during the phase transformations of the precursor materials in this sintered mixture (Drits *et al.*, 2019; Húlan *et al.*, 2019; Karbalaei Saleh *et al.*, 2019; Chalouati *et al.*, 2020; ElDeeb *et al.*, 2020a), three main significant regions of the well-defined weight losses on the TGA curve were considered as the initial (or datum) state for monitoring the thermal changes (i.e. before the addition of charcoal). The AB region occurs at temperatures <200°C, the BC region occurs at 450–650°C and the CD region occurs within the 650–850°C range. On the DSC curve, the first endothermic peak at 111.2°C (corresponding to the AB region) is attributed to the loss of adsorbed water. The second endothermic peak at 507.5°C (corresponding to the BC region with weight loss of 3.27 wt.%) is attributed to the dehydroxylation of kaolinite and its transformation into the highly reactive metakaolinite ($Al_2Si_2O_7$) phase, which facilitated Al_2O_3 extraction in the leaching stage. The third endothermic peak at 844.4°C (corresponding to the CD region with weight loss of 29.69 wt.%) is due to the complete decomposition of calcite in the limestone fraction to the reactive lime (CaO) phase. The sharp exothermic peak at 975.5°C corresponds to the transformation of metakaolinite into the Al–Si spinel phase (and/or a mixture of γ-alumina, amorphous silica and mullite).

The TGA and DSC curves (Fig. 1b,c) indicate the thermal changes accompanied by the additions of charcoal to the kaolin-limestone mixture of 1% and 4%, respectively. After the addition of charcoal to the mixtures, the temperatures of the phase transformations decreased. At 1% charcoal content (Fig. 1b), the DSC endothermic peak of the kaolinite dehydroxylation enthalpy appeared at 494.9°C and that of the complete limestone decomposition in the mixture appeared at 821.2°C. The sharp DSC exothermic peak at 969.6°C indicates the transformation of metakaolinite to the Al-Si spinel (and/or a mixture of γ-alumina, amorphous silica and mullite). At 1% charcoal content (Fig. 1c), the dehydroxylation temperature of kaolinite decreased from 507.5°C to 494.8°C, the temperature limit of the complete limestone decomposition fell from 844.4°C to 811.0°C and the temperature of the transformation of metakaolinite to Al-Si spinel decreased from 975.5°C to 967.3°C. Increasing the charcoal content from 1% to 4% did not lead to significant changes in the thermal behaviour.

Thermodynamically, the thermal changes accompanied by the phase transformations are mainly controlled by the partial pressure of both the water vapour (adsorbed and hydroxyl water in kaolinite) and the CO_2 emitted (from the complete decomposition of calcite). Hence, the excessive pressure may reduce the transformation temperatures with increasing amounts of charcoal, as indicated in Equations 4–7 (Zhou *et al.*, 2012; Yuan *et al.*, 2018; ElDeeb *et al.*, 2020b).

$$C + O_2 \rightarrow CO_2 \quad (4)$$

$$2C + O_2 \rightarrow 2CO \quad (5)$$

$$2CO + O_2 \rightarrow 2CO_2 \quad (6)$$

$$CO_2 + C \rightarrow 2CO \quad (7)$$

In addition, a sharp DSC exothermic peak appeared at 1144.9°C (Fig. 1c), corresponding to the transformation of Al-Si spinel into the dicalcium silicate phase ($2CaO.SiO_2$) according to Equation 8.

$$3Al_2O_3 \cdot 2SiO_2 + 4CaO \rightarrow 2\beta - 2CaO \cdot SiO_2 + 3Al_2O_3 \quad (8)$$

Increasing the charcoal content facilitated the formation of the dicalcium silicate phase ($2CaO.SiO_2$) at a lower temperature (<1200°C). Hence, the added charcoal acted as a fluxing agent and a thermal activator (as indicated by the TGA and DSC analyses) because it accelerated both the dehydroxylation of kaolinite and the decomposition of calcium carbonate and hence accelerated the reaction between the resulting lime and metakaolinite to produce the desired leachable calcium aluminate phase ($C_{12}A_7$).

https://doi.org/10.1180/clm.2022.7 Published online by Cambridge University Press

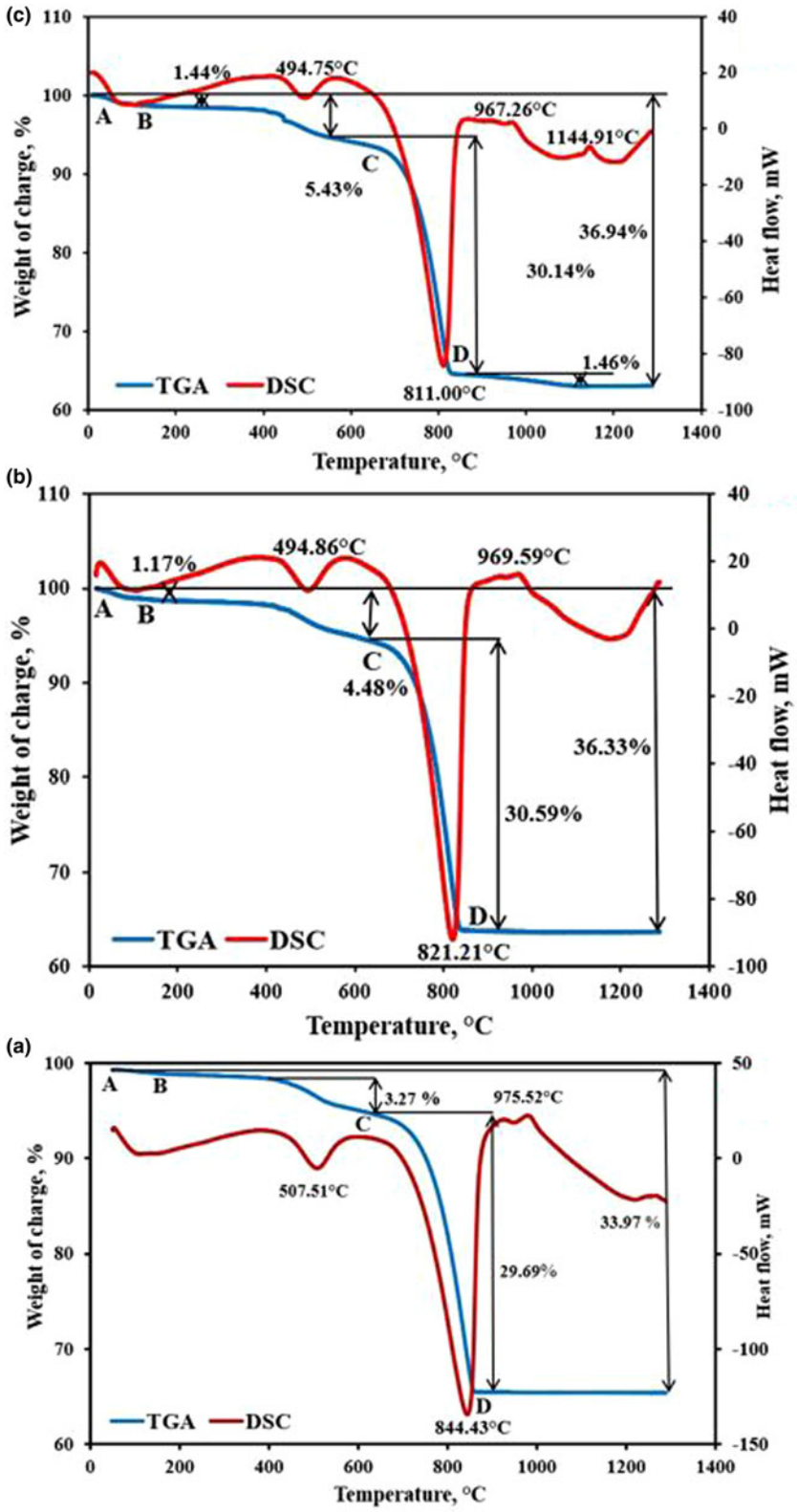

Fig. 1. TGA and DSC curves of limestone-kaolin mixtures with various amounts of charcoal: (a) 0%, (b) 1% and (c) 4%. The regions of well-defined weight losses on the TGA curve were as follows: the **AB** region appeared at temperatures <200°C; the **BC** region emerged at temperatures >450°C; and the **CD** region existed over the range 650–850°C.

Effects of charcoal addition on the phase transformation and microstructure

The phase transformation changes of the sintered kaolin-limestone mixtures at the highest optimum temperature, 1360°C and with variable charcoal contents as indicated by the XRD traces (ElDeeb *et al.*, 2020a) are shown in Fig. 2. In all of the traces, the γ-C_2S phase was identified by the peaks at 29.63 and 47.53°2θ (Jadhav & Debnath, 2011). In the charcoal-free sample, the crystalline calcium aluminate phase ($Ca_{12}Al_{14}O_{33}$) was identified from the peaks at 14.70, 22.50 and 23.22°2θ (Zhang *et al.*, 2015a) and the crystalline aluminosilicate phase (Al_2SiO_5) was

https://doi.org/10.1180/clm.2022.7 Published online by Cambridge University Press

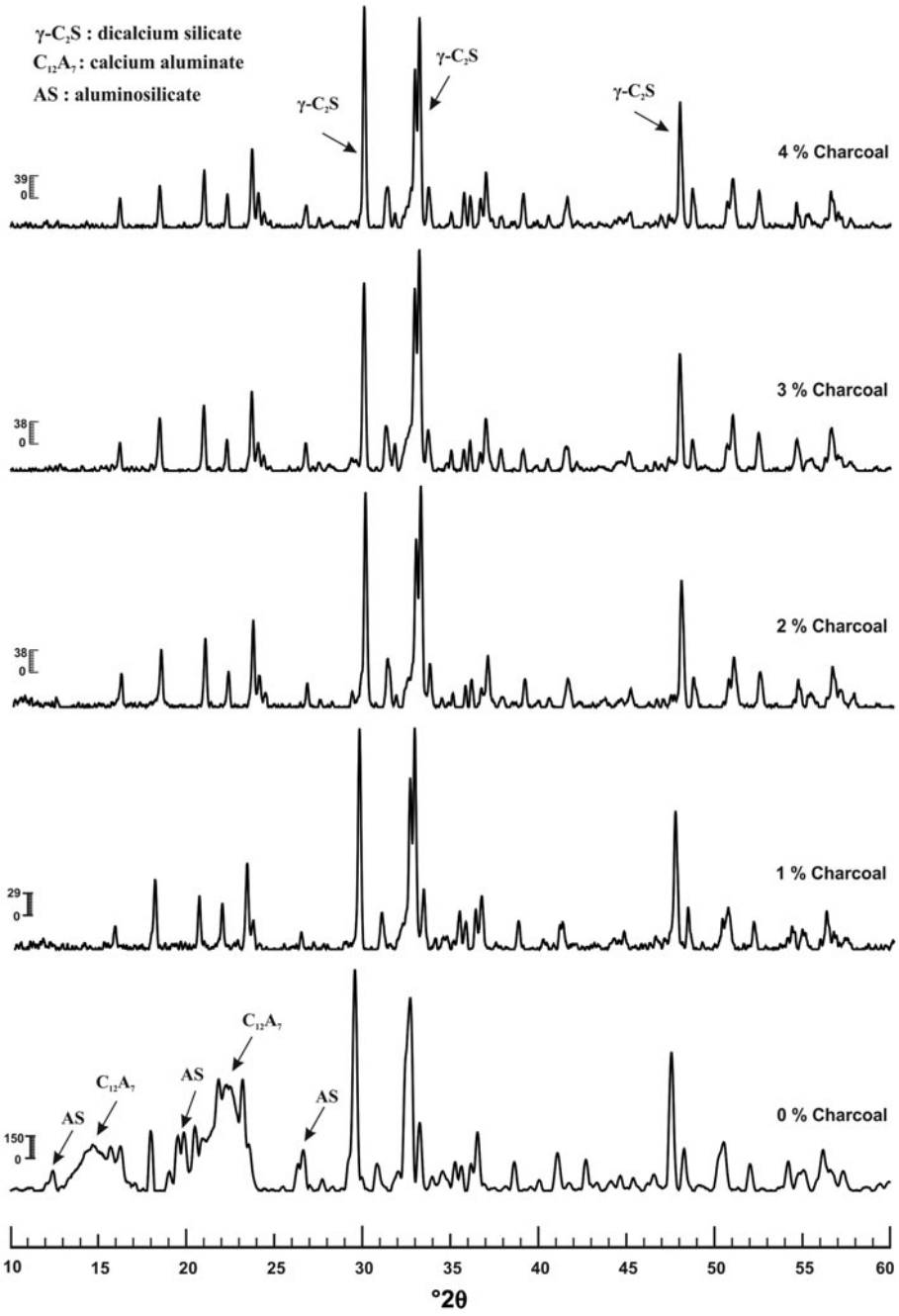

Fig. 2. XRD traces showing phase transformations in the sintered limestone-kaolin mixtures with variable amounts of charcoal (0–4%) at the optimum temperature of 1360°C.

identified from the peaks at 12.40°2θ, 19.50°2θ and 26.66°2θ (ElDeeb *et al.*, 2020b). In samples with added charcoal (1–4%), under the same sintering conditions, the aluminosilicate and calcium aluminate phases disappeared as they transformed into amorphous phases (Fig. 2). The resulting amorphous calcium aluminate phase is a highly desirable and effective component causing significant Al_2O_3 leachability and therefore improved APR (ElDeeb *et al.*, 2020a). In addition, the predominance of a crystalline dicalcium silicate phase increased the efficiency of the self-integration process in all of the resulting charcoal-activated sinters. Hence, the targeted thermochemical amorphization by the addition of charcoal yielded greater chemical reactivity and more efficient leachability in the dilute alkaline solutions than sintering without the addition of charcoal (Liew *et al.*, 2012; Zhou *et al.*, 2012; Li *et al.*, 2014b; Xu *et al.*, 2015; D'Elia *et al.*, 2018; Yuan *et al.*, 2018; ElDeeb *et al.*, 2019, 2020a, 2020b). Moreover, the addition of charcoal had a significant effect on the surface properties and degree of disorder of the sintered components, which facilitated their transformations into the final amorphous material (Yuan *et al.*, 2018).

The abundance of the resulting crystalline calcium silicates (and hence the extent of their self-disintegration) increased with increasing sintering temperature; hence, the frequency of the separate finer particles in the resulting loose calcium aluminate fraction increased significantly (ElDeeb *et al.*, 2020a). Figure 3 shows the general microtextural and micromorphological changes in the resulting sinters in the temperature range 1260–1360°C with the addition of the optimum 1.5% charcoal content. Normally, the

https://doi.org/10.1180/clm.2022.7 Published online by Cambridge University Press

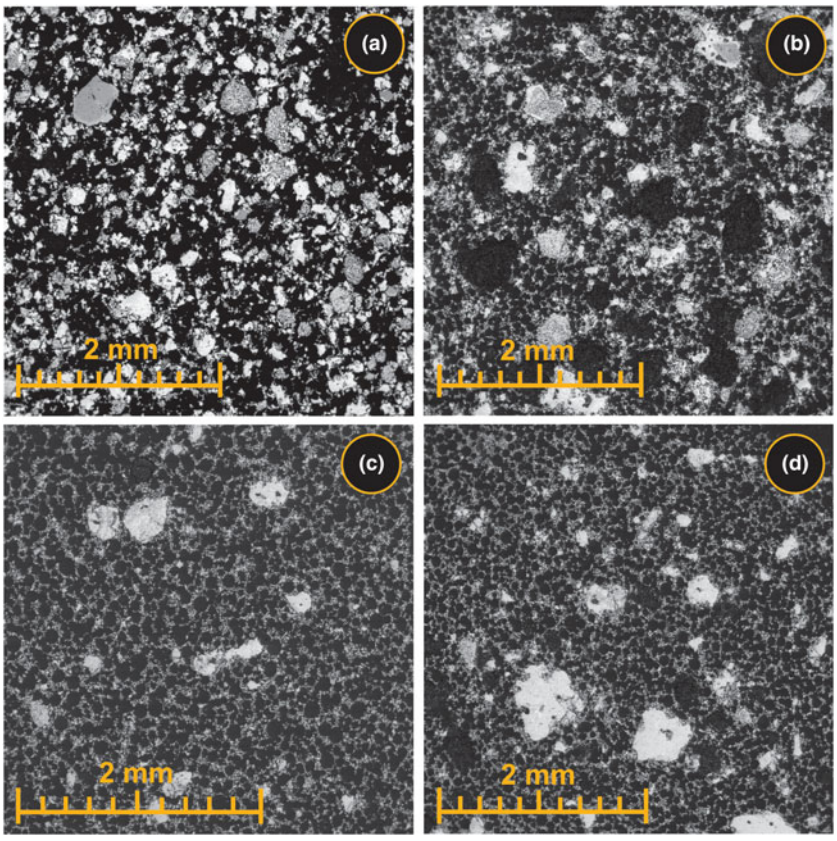

Fig. 3. Back-scattered electron images of the sinters produced at (a) 1260°C, (b) 1300°C, (c) 1340°C and (d) 1360°C with the addition of 1.5% charcoal.

sizes of the self-disintegrated particles decrease with increasing sintering temperature (ElDeeb *et al.*, 2020a); hence, the resulting sinters under the high-temperature limits of 1340°C and 1360°C consisted of finer calcium aluminate particles that aggregated as a groundmass matrix (mainly particle sizes <10 μm; Fig. 3c,d) than those produced under lower temperatures of 1260°C and 1300°C (with particle sizes >50 μm and up to 1 mm; Fig. 3a,b).

Moreover, under a relatively low temperature (1260°C), with the addition of 1.5% charcoal, a small amount of non-reactive relict crystals composed of the precursor kaolinite and calcite components as well as secondary SiO_2 and Al_2O_3 remained in the sinter (Fig. 4a). As the temperature increased to 1360°C, the abundance of these relicts decreased significantly (Fig. 4b) due to kaolinite dehydroxylation and limestone decomposition and their transformation into the highly reactive metakaolinite and lime phases. Then, the highly self-disintegrated crystalline calcium silicate and the easily leachable amorphous calcium aluminate phases were formed, which were effective at increasing the magnitude of the APR. Therefore, a high sintering temperature in the presence of charcoal led to a combination of favourable phase changes with desirable micrometric characteristics in the resulting sinter that effectively increased the APR.

Figure 5 shows the distributions of Si and Al atoms within a typical multiphase particle in the resulting sinter at 1360°C with the addition of 1.5% charcoal. The calcium aluminate phase was mainly concentrated in the inner zone of the particle surrounded by finer aggregates of the calcium silicate and aluminosilicate phases. After leaching of the highest-temperature sinter (1360°C with 1.5% charcoal), the calcium aluminate phase was concentrated mainly in the inner zones (i.e. the core) of the resulting multiphase sludge particles. In some particles, the calcium aluminate phase was surrounded by the non-leachable silicate and aluminosilicate phases that existed as finer aggregates in the peripheral zones (i.e. the crust; Fig. 6). Moreover, in some other particles, the aluminate phase (i.e. the large, light grey areas) was covered by dense carbonate masses (i.e. the dark grey rim) that precipitated during the leaching process (Fig. 6b,c). The diffused crystalline calcium silicate crust that covered the sludge particles probably acted as a barrier, affecting the complete dissociation of the Al_2O_3 (i.e. 100% APR) from the aluminate phases in the sludge during leaching (ElDeeb *et al.*, 2020a).

In the microstructure, the transformed amorphous and crystalline multiphase components in both the sinter (produced at 1360°C with 1.5% charcoal) and its related sludge can be distinguished from their average EDX microchemical compositions (Table 3). The transformed components in the resulting charcoal-activated sinter at 1360°C (Figs 2, 4b & 5) were distinguished into five phases: the calcium aluminate type (I), the calcium aluminate type (II), the aluminosilicate type (I), the aluminosilicate type (II) and the dicalcium silicate. Despite their absence from the XRD traces (Fig. 2), the two types of amorphous calcium aluminates (I and II) were confirmed by the greatest average Al contents of 17.7–24.2% with relatively high Ca contents of 36.3–43.9% and the smallest average Si contents of 0.3–1.4%. In addition, they contained Na ≤0.2%, K ≤0.3%, Mg contents ≤0.4% and Fe ≤1.2% on average. The amorphous aluminosilicate phases (I and II) showed average Al contents of 12.5–18.1%, Si contents of 2.3–14.3% and lower average Ca contents (28.0–30.0%) than the amorphous calcium aluminates. Moreover, they had the greatest average Mg contents (1.4–9.6%), average Fe contents up to 1.5% and Na and K contents up to 0.8%. The crystalline C_2S phase had the smallest Al contents among all the five phases, with an average of 0.5%, but it exhibited the greatest average Ca and Si contents of 46.8% and 15.6%, respectively. In addition, it had the

https://doi.org/10.1180/clm.2022.7 Published online by Cambridge University Press

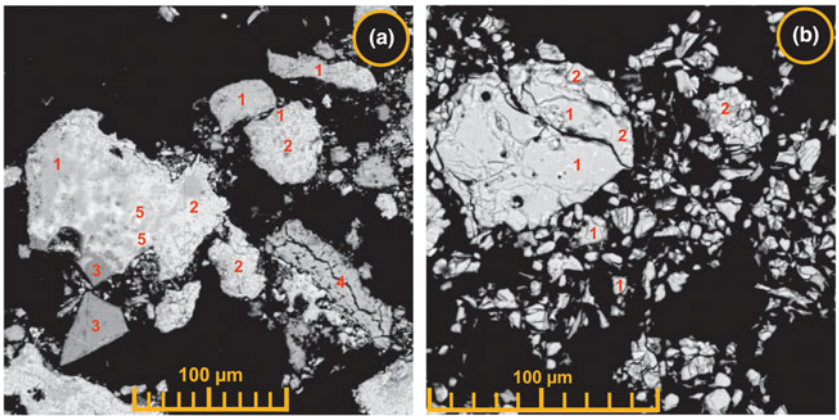

Fig. 4. Back-scattered electron images showing the microstructural characteristics of the sinters produced at (a) 1260°C and (b) 1360°C with the addition of 1.5% charcoal. 1 = calcium aluminates; 2 = calcium silicates; 3 = relicts of kaolin/SiO_2; 4 = free CaO; 5 = structurally non-free CaO.

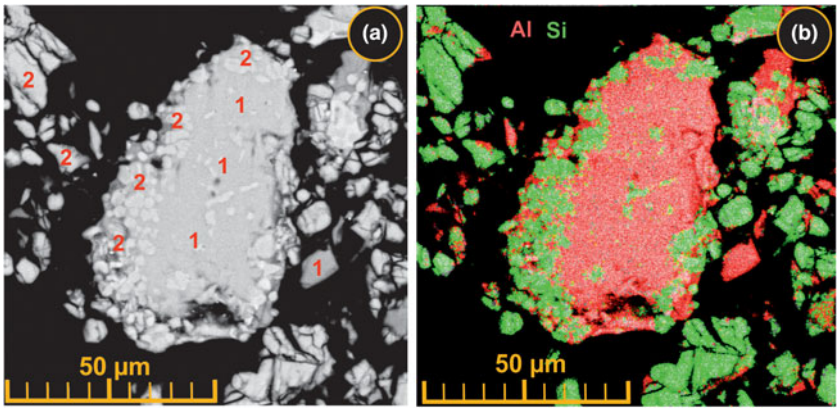

Fig. 5. (a) Back-scattered electron image showing a typical multiphase particle of the sinter produced at 1360°C with 1.5% added charcoal. 1 = calcium aluminate phases; 2 = calcium silicate and aluminosilicate phases. (b) Elemental modal map showing the distributions of Al and Si on a typical multiphase particle of the sinter produced at 1360°C.

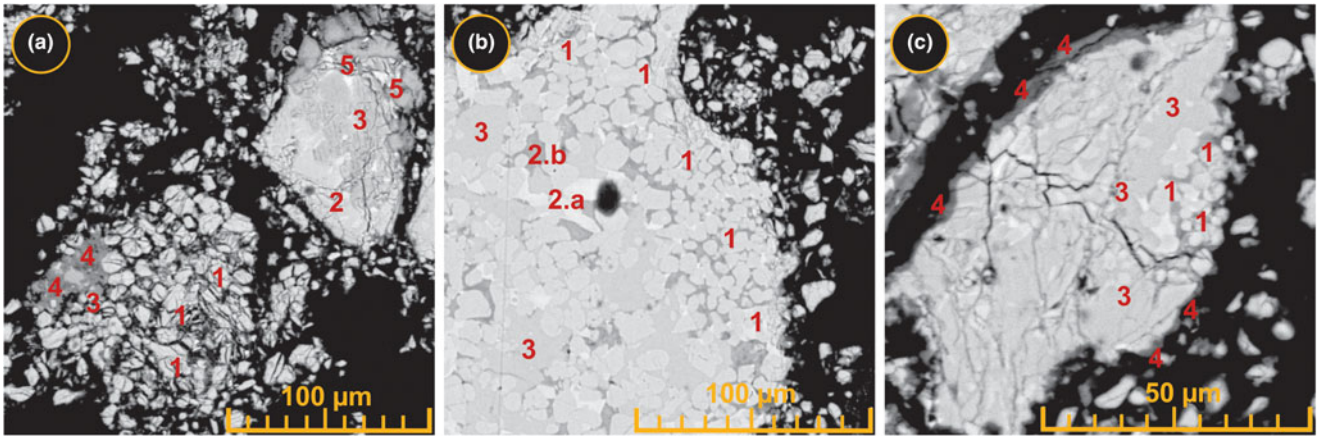

Fig. 6. Back-scattered electron images showing the microstructural characteristics of the sludge resulting from the leaching process of the sinter produced at 1360°C with the addition of 1.5% charcoal. (a) Morphology of leached self-disintegrated particles in the sludge sample. (b) The distribution of calcium silicates within the microtexture of the leached sludge particles. (c) Calcium carbonate deposition on the outer peripheries of the deformed (cracked) sludge particles after leaching. 1 = calcium silicates; 2.a = aluminosilicate type I, 2.b = aluminosilicate type II; 3 = calcium aluminates; 4 = calcium carbonate; 5 = calcium oxide.

smallest average contents of both Mg and Fe that did not exceed 0.1% and was free of alkali metals (Na and K). However, the chemical composition of the sludge was similar to its precursor sinter, which also reflected the same multiphase components of the amorphous aluminosilicate and calcium aluminate phases as well as the crystalline C_2S phase (Table 3).

The small SiO_2 contents (≤2%) of the leachable calcium aluminate phases in the sinter reflect the high sintering quality that led to greater alumina leachability from the sludge during the hydrometallurgical processing (Mejía De Gutiérrez *et al.*, 2008; Azof *et al.*, 2019, 2020). In the studied sinters, the leachable calcium aluminate phases I and II had small SiO_2 contents (≤1.5%; Table 3); hence, the residual calcium aluminates in the resulting sludge had small Al contents (18.1%; Table 3). The small Al contents in the resulting sludge indicate an increased extent of Al dissociation, resulting in a high APR. In addition, the Al-containing phases did not completely release the total Al_2O_3 content during the leaching process because of the

https://doi.org/10.1180/clm.2022.7 Published online by Cambridge University Press

Table 3. Elemental composition from the EDX analysis ($n = 10$) of the sinter produced at 1360°C with 1.5% added charcoal and its sludge produced by the leaching process.

Sample	Components	Composition (wt.%)							
		Value	Na	Mg	Al	Si	K	Ca	Fe	O
Sinter	Calcium aluminate (type I)	Average	–	0.3	17.7	1.4	–	43.9	1.2	36.0
		Maximum	0.1	0.4	18.1	2.1	0.1	44.7	1.4	36.0
		Minimum	–	0.2	17.3	1.0	–	43.5	0.9	35.0
	Calcium aluminate (type II)	Average	0.2	0.4	24.2	0.3	0.3	36.3	1.0	37.0
		Maximum	0.3	0.6	25.9	1.1	0.6	43.7	1.3	38.0
		Minimum	0.1	0.3	18.1	0.1	–	34.2	0.9	36.0
	Calcium silicate	Average	–	0.1	0.5	15.6	–	46.8	0.1	37.0
		Maximum	0.1	0.1	1.0	16.2	–	47.0	0.2	37.0
		Minimum	–	–	–	15.4	–	46.2	–	37.0
	Aluminosilicate (type I)	Average	0.2	9.6	18.1	2.3	0.5	30.0	1.5	38.0
	Aluminosilicate (type II)	Average	0.8	1.4	12.5	14.3	0.8	28.0	1.5	41.0
		Maximum	1.5	2.7	15.1	17.5	1.8	28.5	2.0	41.0
		Minimum	0.5	0.7	7.8	12.8	0.3	26.9	1.2	40.0
Sludge	Calcium aluminate	Average	0.1	0.3	18.1	1.2	–	43.9	1.0	36.0
		Maximum	0.1	0.3	18.3	1.4	–	44.4	1.3	36.0
		Minimum	–	0.2	17.8	1.0	–	43.5	0.8	35.0
	Calcium silicate	Average	–	–	–	16.1	–	46.8	–	37.0
		Maximum	–	0.1	0.1	16.2	–	47.0	0.1	37.0
		Minimum	–	–	–	16.0	–	46.7	–	37.0

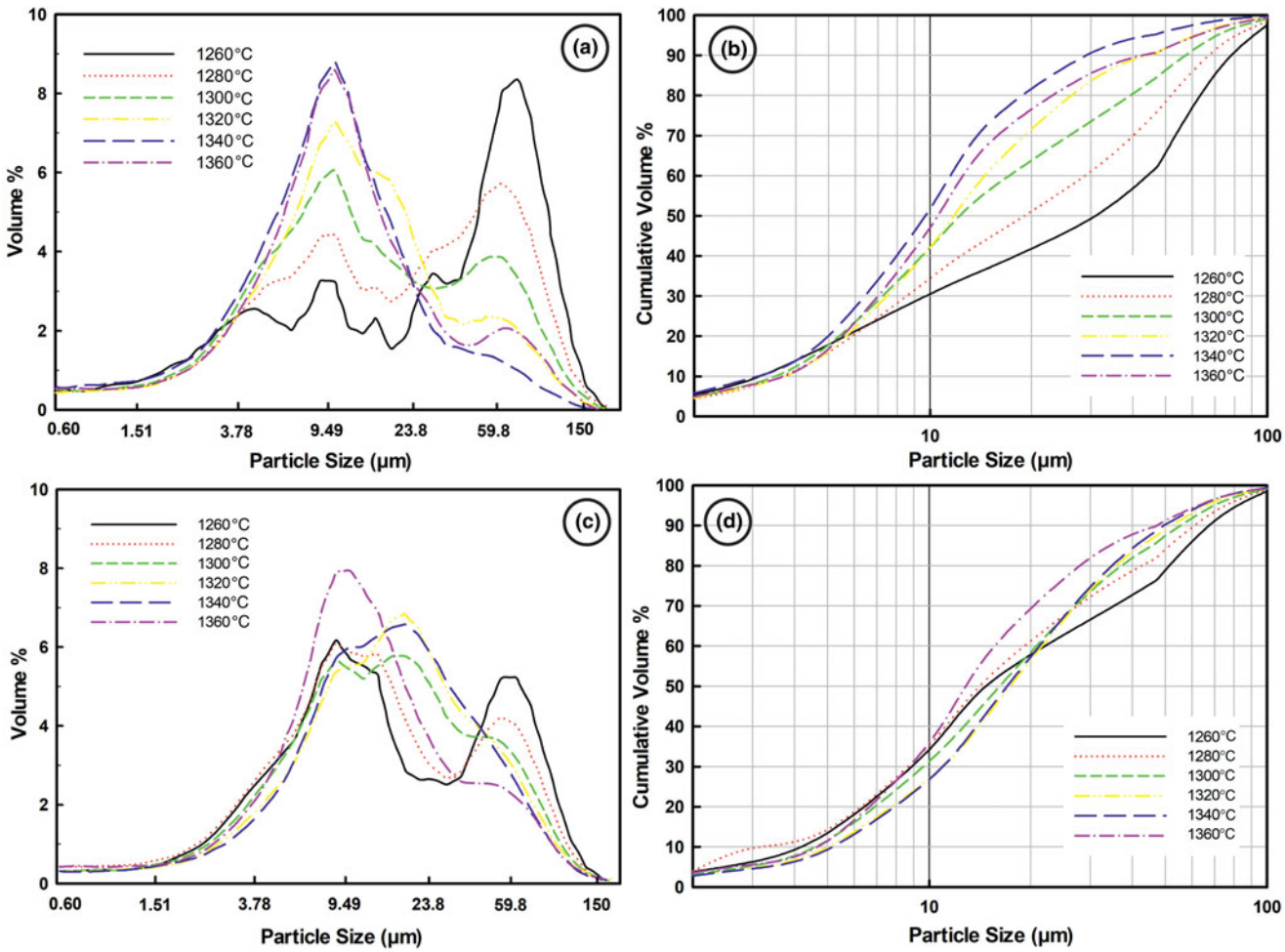

Fig. 7. Effects of sintering temperature within the range 1260–1360°C on the particle-size distribution with the addition of 1.5% charcoal: (a) frequency curves and (b) cumulative curves of the sinters; (c) frequency curves and (d) cumulative curves of the related sludges obtained after the leaching process.

https://doi.org/10.1180/clm.2022.7 Published online by Cambridge University Press

Table 4. Particle-size distributions ($n = 3$) of the sintered kaolin-limestone mixtures under variable temperatures within the range 1260–1360°C with the addition of 1.5% charcoal (SD = ±2).

	Particle size (μm)										Size homogeneity and gradation parameters		
Sintering temperature (°C)	Fine fraction (<1 μm)	D_{10}	D_{20}	D_{30}	D_{40}	D_{50}	D_{60}	D_{70}	D_{80}	D_{90}	Span	C_u	C_c
1260	0.49%	3.1	5.7	9.8	18.7	31.0	44.2	53.9	63.8	77.6	2.40	14.26	0.70
1280	0.49%	3.6	6.0	8.7	12.2	19.5	28.9	40.0	52.0	67.3	3.27	8.03	0.73
1300	0.51%	3.4	5.4	7.4	9.5	12.2	16.9	25.5	39.5	57.0	4.39	4.97	0.95
1320	0.55%	3.6	5.8	7.7	9.6	11.7	14.6	18.5	25.1	44.6	3.50	4.06	1.13
1340	0.59%	3.1	5.0	6.6	8.2	9.70	11.5	13.9	18.0	28.4	2.61	3.71	1.22
1360	0.63%	3.6	5.7	7.4	8.9	10.5	12.5	15.9	23.6	43.7	3.82	3.47	1.22
R^2 (*vs* sintering temperature)	0.93	–	–	0.71	0.70	0.74	0.79	0.86	0.88	0.80	–	0.75	0.93

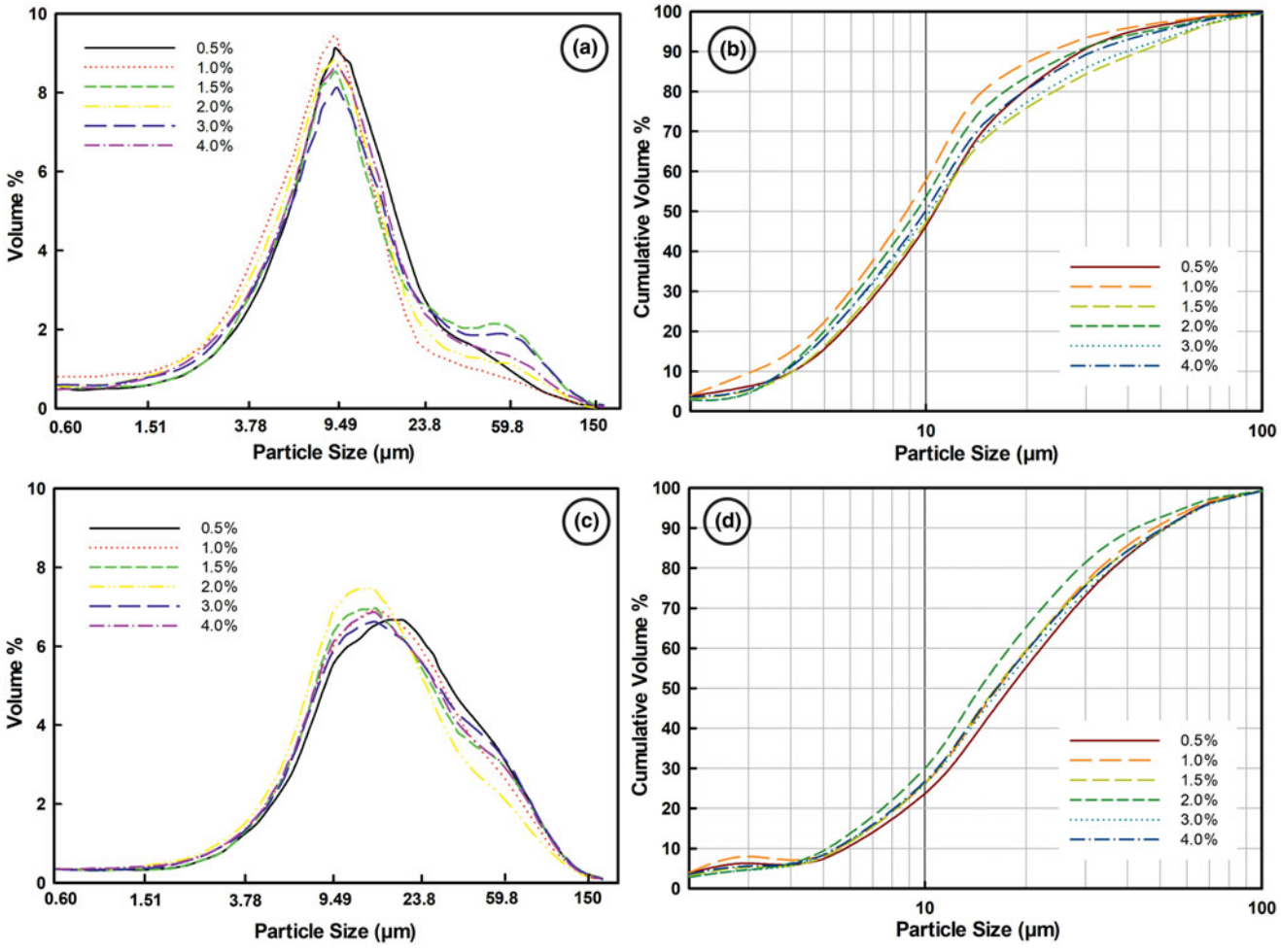

Fig. 8. Effects of added charcoal percentage (0.5–4.0%) on the particle-size distribution at a fixed sintering at 1360°C: (a) frequency curves and (b) cumulative curves of the sinters; (c) frequency curves and (d) cumulative curves of the related sludges obtained after the leaching process.

significant Si contents (>2%) in the aluminosilicates (i.e. up to 14.3%; Table 3).

Effects of charcoal thermochemical activation on self-disintegration efficiency

The particle-size characteristics of the sinter are key factors in the leaching process during Al_2O_3 extraction from the sintered kaolin-limestone mixture. The finer the particle size of the sinter powder, the greater the leaching rate of Al_2O_3 and hence the greater the resulting APR (ElDeeb *et al.*, 2020a). Particle self-disintegration *via* the sintering of kaolin-limestone mixtures at <1360°C was the most important process for the intrinsic size reduction in the resulting sinter powders, and hence it is considered to be a cost-effective and energy-efficient factor to help avoid pre-leach grinding. The self-disintegration process normally takes place due to the formation of the crystalline β-C_2S ($2CaO{\cdot}SiO_2$) under high temperatures and then its transformation into the

https://doi.org/10.1180/clm.2022.7 Published online by Cambridge University Press

Table 5. Particle-size distributions ($n = 3$) of the sintered kaolin-limestone mixtures under variable amounts of additional charcoal (0–4%) and a sintering temperature of 1360°C (SD = ±2).

Amount of charcoal added (%)	Particle size (μm)										Size homogeneity and gradation parameters		
	Fine fraction (<1 μm)	D_{10}	D_{20}	D_{30}	D_{40}	D_{50}	D_{60}	D_{70}	D_{80}	D_{90}	Span	C_u	C_c
0.5	0.55%	3.71	5.86	7.57	9.07	10.6	12.3	14.8	18.7	28.5	2.34	3.31	1.26
1.0	0.80%	2.70	4.62	6.13	7.55	8.92	10.3	12.1	14.8	21.6	2.12	3.81	1.35
1.5	0.57%	3.63	5.68	7.37	8.90	10.5	12.5	15.9	23.6	43.7	3.81	3.44	1.20
2.0	0.55%	3.05	4.96	6.57	8.04	9.47	11.1	13.2	16.7	27.5	2.58	3.64	1.27
3.0	0.60%	3.19	5.24	7.00	8.62	10.3	12.3	15.3	21.4	40.2	3.59	3.86	1.25
4.0	0.48%	3.23	5.27	6.95	8.47	9.99	11.8	14.2	18.4	31.6	2.84	3.65	1.27

γ phase (Fig. 2) during the cooling of the sintered mixture according to Equations 9 & 10 (ElDeeb *et al.*, 2020a).

$$2CaO + SiO_2 \xrightarrow{1145^\circ C} \beta\text{-}Ca_2SiO_4 \quad (9)$$

$$\beta\text{-}Ca_2SiO_4 \xrightarrow{675^\circ C} \gamma\text{-}Ca_2SiO_4 \quad (10)$$

The self-disintegration process of sintered kaolin-limestone mixture without addition of charcoal was initiated at high temperatures of 1300–1400°C (ElDeeb *et al.*, 2019, 2020a). Charcoal was seen to be a thermal activator even in small amounts (0.5%) as self-disintegration was effectively initiated at 1260°C. With the addition of charcoal at the optimum content of 1.5%, the resulting sinters showed a significant size reduction with increasing sintering temperature from 1260 to 1360°C (Fig. 7a,b & Table 4). The finest particle sizes were observed in the sinter powder produced at 1340°C (median $D_{50} = 9.7$ μm), while the lowest sintering temperature of 1260°C produced a powder with of $D_{50} = 31$ μm. The amounts of the finest fractions in the self-disintegrated particles (<1 μm) of the sinters showed a strong positive correlation with sintering temperature ($R^2 = 0.93$; Table 4). The <1 μm fractions increased from 0.49% (sintering at the lowest temperature of 1260°C) to 0.63% (sinters produced at the highest temperature of 1360°C). The sinter produced at 1340°C showed a unimodal distribution, while the particle-size distributions of the remaining sinters were bimodal (Fig. 7a). The specific parameters of the particle-size homogeneity (span $= (D_{90} - D_{10})/D_{50}$), the uniformity coefficient ($C_u = D_{60}/D_{10}$) and the gradation curvature coefficient ($C_c = D_{30}^2/(D_{60}D_{10})$) were calculated (Table 4) (Awad *et al.*, 2018a, 2020). There was no significant correlation between sintering temperature and the particle-size homogeneity of any of the sinters, as the size span values ranged from 2.40 (in the sinter produced under 1260°C) to 4.39 (in the sinter produced under 1300°C), with an average value of 3.33. Sintering temperature showed a strong positive correlation ($R^2 = 0.93$) with the curvature coefficient (C_c) and a significant negative correlation ($R^2 = -0.75$) with the uniformity coefficient (C_u). The C_c values being >1 indicated that the sinters produced at 1320–1360°C consisted of well-graded particles, while the sinters produced at temperatures of ≤1300°C consisted of poorly graded particles with C_c values of <1 (Awad *et al.*, 2018a). Despite the finer particle size of the precursor sinter produced at 1340°C, the resulting related sludge had a larger particle size with $D_{50} = 17$ μm (Fig. 7c,d). This can be attributed to the precipitation of $CaCO_3$ onto the surfaces of the residual non-leachable components. The secondary agglomeration of the fine $CaCO_3$ particles was the most plausible mechanism to explain the particle-size enlargement when compared to the coarser $CaCO_3$ particles that formed *via* primary crystal growth (Azof & Safarian, 2020; Azof *et al.*, 2019, 2020; ElDeeb *et al.*, 2020a).

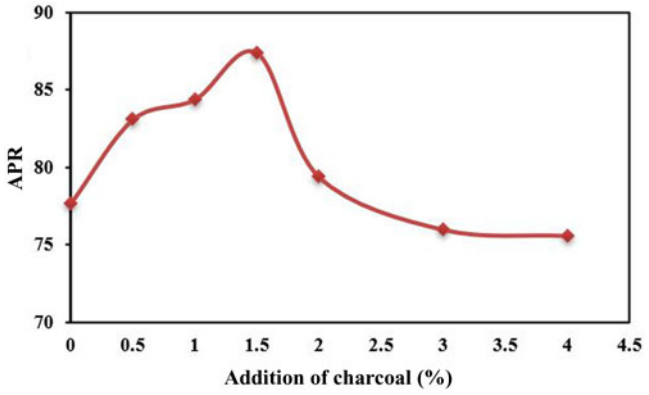

Fig. 9. Effects of the variable amounts of charcoal added (0–4%) on the APR of kaolin-limestone-charcoal mixtures sintered at 1360°C.

Using 1360°C as the optimum sintering temperature, charcoal contents of 0.5–4.0% (Fig. 8 & Table 5) showed significant stability in terms of the improved self-disintegration efficiency of the resulting sinters compared to sintering at 1360°C with 1.5% charcoal (Table 5). This is indicated by the median D_{50} values that ranged between 8.9 μm (1% charcoal content) and 10.6 μm (0.5% charcoal content), with an average of 10 μm. The fine fractions (<1 μm) ranged between 0.55% and 0.80% (1% charcoal content), with an average of 0.59%. In addition, the size span values ranged between 2.1 and 3.8, with an average of 2.9, and the C_c values ranged between 1.2 and 1.4, with an average of 1.3 (Table 5).

Effects of charcoal thermochemical activation on APR

As the optimum sintering temperature to produce the greatest APR was 1360°C (ElDeeb *et al.*, 2019, 2020a), the effects of the varied amounts of added charcoal in the kaolin-limestone mixture on the APR were examined at that temperature. By increasing the amount of charcoal added from 0.5% to the optimum 1.5%, the APR increased gradually from 77.7% to 87.4% (Fig. 9). With further addition of charcoal, up to 4%, the APR gradually decreased from 87.4% to 75.6%. This is attributed to the release of excessive

https://doi.org/10.1180/clm.2022.7 Published online by Cambridge University Press

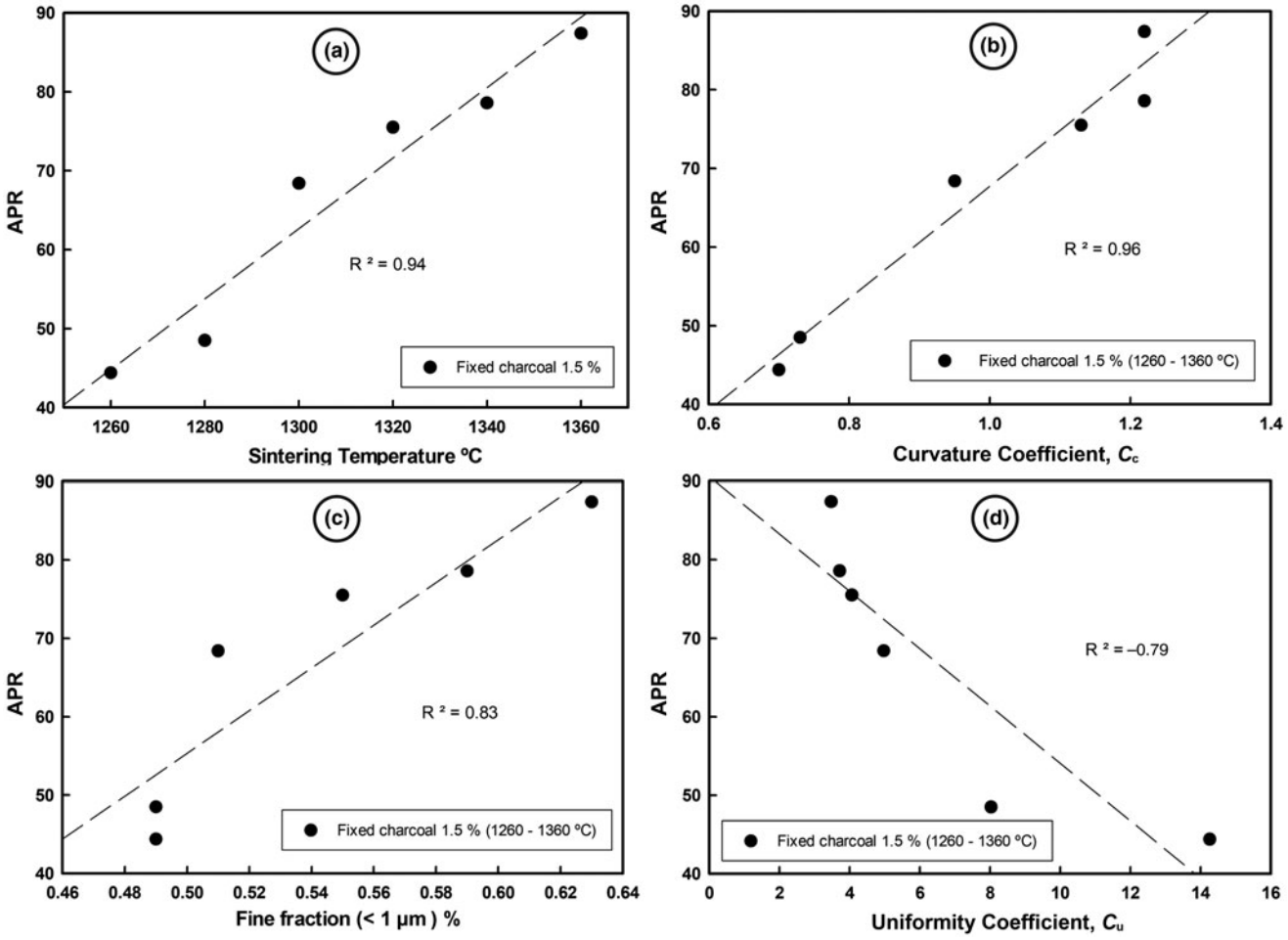

Fig. 10. Effects of the variable sintering temperatures (1260–1360°C) and the size-distribution parameter on the APR with the addition of 1.5% charcoal: (a) the effect of sintering temperature on the APR; (b) correlation between the APR and size-curvature coefficient, C_c; (c) correlation between the APR and fine fraction (<1 µm); and (d) correlation between the APR and size uniformity coefficient, C_u.

heat by the larger amounts of charcoal, which led to the formation of mullite, from which Al_2O_3 is leached with difficulty.

Sintering temperature was the main factor controlling the phase transformations and microstructural changes that drove the self-disintegration process and hence significantly increased the APR (ElDeeb *et al.*, 2019, 2020b). At the same optimum amount of charcoal added, 1.5%, the resulting APR values were strongly correlated with sintering temperature ($R^2 = 0.94$), as the APR values increased gradually from 44.4% for sintering at 1260°C to 87.4% for sintering at 1360°C (Fig. 10a). As sintering temperature had a significant effect on the particle-size distribution (Fig. 7 & Table 4), the resulting APR showed a strong positive correlation ($R^2 = 0.96$) with the curvature coefficient, C_c (Fig. 10b). The APR showed a positive correlation ($R^2 = 0.83$) with the fine fraction (<1 µm) contents (Fig. 10c) and a negative correlation ($R^2 = -0.79$) with the uniformity coefficient, C_u (Fig. 10d). Thus, a sintering temperature of 1360°C and the addition of 1.5% charcoal were the optimum conditions for the formation of highly leachable amorphous calcium aluminate ($C_{12}A_7$) according to Equations 11 & 12. In addition, crystalline C_2S was the most efficient self-disintegration controlling phase in the resulting sinters, as is indicated by the increase in the particle fine fraction contents and the influence on the particle-size gradation. Sintering at a lower temperature (1260°C) was insufficient for complete formation of the $C_{12}A_7$ and C_2S phases.

$$Al_2O_3 + CaO \rightarrow CaO \cdot Al_2O_3 \quad (11)$$

$$7Al_2O_3 + 12CaO \rightarrow 12CaO \cdot 7Al_2O_3 \quad (12)$$

In the case of sintering at 1360°C without added charcoal, the precursor components reacted and transformed completely into the leachable calcium aluminate phase ($C_{12}A_7$). The additional heat generated under these conditions facilitated the crystallization of the calcium aluminate phase (ElDeeb *et al.*, 2019, 2020b, 2020c, 2021). The addition of charcoal up to 1.5% increased total heat during the transformation due to the combustion of charcoal in this closed system (as is indicated by the significant thermal changes on the DSC curves; Fig. 1). These conditions caused amorphization of the calcium aluminate phase (cf. Figs 2 & 5), yielding fine self-disintegrated particles and surface properties, which led to enhanced leachability and greater Al_2O_3 production. However, the decreasing APR with charcoal contents >1.5% is attributed to the release of an excessive heat, producing mullite, from which alumina is extracted with difficulty (Qiao *et al.*, 2008; ElDeeb *et al.*, 2020b).

https://doi.org/10.1180/clm.2022.7 Published online by Cambridge University Press

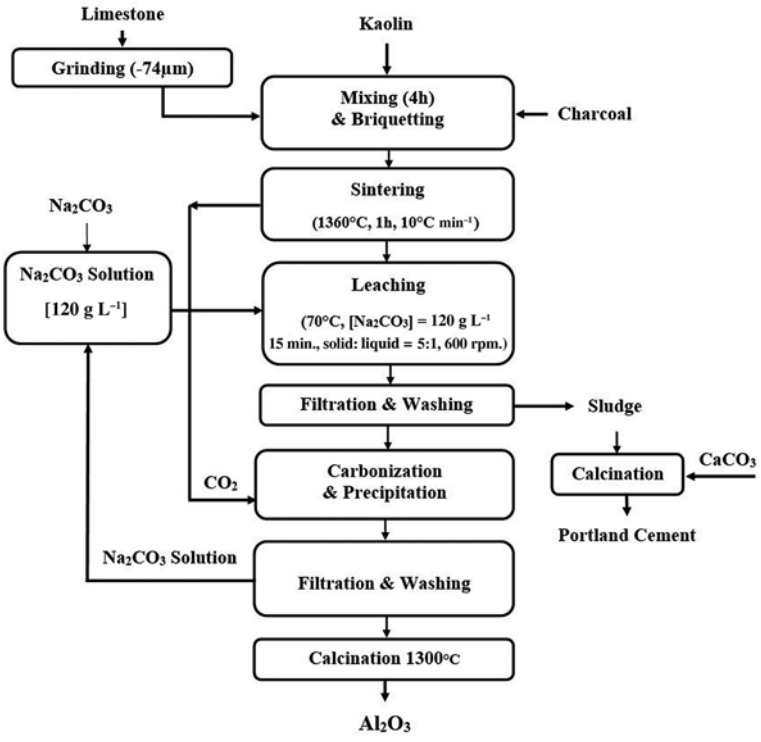

Fig. 11. The proposed flow diagram for the pyro-hydrometallurgical processing of kaolin ore using the lime-sintering process for Al_2O_3 extraction.

Therefore, the charcoal content of 1.5% was optimal for sintering at 1360°C to produce the greatest APR. The main advantages of using charcoal instead of other inorganic fluxing materials are the chemical inertness of carbon (i.e. it does not react with the lime and metakaolinite) and the complete loss of the added charcoal mass on ignition. Other known fluxing agents are highly reactive materials (even when added in trace amounts) with the transformed aluminosilicate and lime phases, leading to undesirable intermediate products that decrease alumina leachability and reduce the APR (Pontikes *et al.*, 2010; Wang *et al.*, 2011, 2017; Yu *et al.*, 2012, 2014, 2019). The recommended flow diagram for the pyro-hydrometallurgical processing of kaolin ore to produce alumina using the lime-sintering process with the addition of charcoal is shown in Fig. 11.

Summary and conclusions

Thermochemical activation of kaolin-limestone feeds (e.g. low-grade, non-bauxitic, hydrous, aluminium silicate-rich raw geomaterials) *via* the addition of charcoal is an important process for increasing the APR during pyro-hydrometallurgical processing *via* the lime-sintering process. The present study determined the optimum conditions for this charcoal-based activation and explained the related phase-transformation mechanisms that control the cost-effectiveness and energy efficiency of Al_2O_3 production and of increasing the APR. The study investigated the thermal activation effects of the charcoal on the efficiency of Al_2O_3 extraction from a processed kaolin in the sintering temperature range of 1260–1360°C. The charcoal added to the kaolin-limestone mixture was 0.5–4.0 wt.%. In comparison to relevant previous work by the same authors, the addition of 1.5% charcoal for sintering at 1360°C yielded the maximum APR of 87.4% under the same leaching conditions. Sintering at 1360°C and the addition of ≤1.5% charcoal were the optimum conditions for amorphization of the resulting highly leachable calcium aluminate phase. In addition, the high self-disintegration efficiency explained the high Al_2O_3 leachability of the resulting sinters and therefore the increased APR. Sintering at higher temperatures (>1360°C) and/or with the addition of greater charcoal contents (>4%) produced excessive heat and yielded mullite, from which alumina is leached with difficulty, thereby significantly decreasing the APR. Unlike other inorganic fluxing and activation agents, charcoal is a promising activator for Al_2O_3 production from low-grade raw geomaterials due to its effectiveness at increasing the APR and the stability of its self-disintegration process at lower sintering temperatures, even with the smallest addition of charcoal.

Supplementary material. To view supplementary material for this article, please visit https://doi.org/10.1180/clm.2022.7.

Financial support. The work was carried out with the financial support of the Russian Science Foundation under Agreement No. 18-19-00577 of 28 April 2021 of a grant for fundamental scientific research and exploratory scientific research.

References

Ajemba R.O. & Onukwuli O.D. (2012) Process optimization of sulphuric acid leaching of alumina from Nteje clay using central composite rotatable design. *International Journal of Multidisciplinary Sciences and Engineering*, **3**, 1–7.

Al-Ajeel A.W.A., Abdullah S.Z., Muslim W.A., Abdulkhader M.Q., Al-Halbosy M.K. & Al-Jumely F.A. (2014) Extraction of alumina from Iraqi colored kaolin by lime-sinter process. *Iraqi Bulletin of Geology Mining*, **10**, 109–117.

Al-Zahrani A.A. & Abdul-Majid M.H. (2009) Extraction of alumina from local clays by hydrochloric acid process. *Journal of King Saud University – Engineering Sciences*, **20**, 29–41.

Aldabsheh I., Khoury H., Wastiels J. & Rahier H. (2015) Dissolution behavior of Jordanian clay-rich materials in alkaline solutions for alkali activation purpose. Part I. *Applied Clay Science*, **115**, 238–247.

Allegretta I., Pinto D. & Eramo G. (2016) Effects of grain size on the reactivity of limestone temper in kaolinite clay. *Applied Clay Science*, **126**, 223–234.

Awad M.E., López-Galindo A., Sánchez-Espejo R., El-Rahmany M.M. & Viseras C. (2018a) Thermal properties of some Egyptian kaolin pastes for pelotherapeutic applications: influence of particle geometry on thermal dosage release. *Applied Clay Science*, **160**, 193–200.

Awad M.E., López-Galindo A., Sánchez-Espejo R., Sainz-Díaz C.I., El-Rahmany M.M. & Viseras, C. (2018b) Crystallite size as a function of kaolinite structural order-disorder and kaolin chemical variability: sedimentological implication. *Applied Clay Science*, **162**, 261–267.

Awad M.E., López-Galindo A., Medarević D., Đuriš J., El-Rahmany M.M., Ibrić S. & Viseras C. (2020) Flow and tableting behaviors of some Egyptian kaolin powders as potential pharmaceutical excipients. *Minerals*, **10**, 23.

Azof F.I. & Safarian J. (2020) Leaching kinetics and mechanism of slag produced from smelting-reduction of bauxite for alumina recovery. *Hydrometallurgy*, **195**, 105388.

Azof F.I., Yang Y., Panias D., Kolbeinsen L. & Safarian J. (2019) Leaching characteristics and mechanism of the synthetic calcium-aluminate slags for alumina recovery. *Hydrometallurgy*, **185**, 273–290.

Azof F.I., Vafeias M., Panias D. & Safarian J. (2020) The leachability of a ternary $CaO–Al_2O_3–SiO_2$ slag produced from smelting-reduction of low-grade bauxite for alumina recovery. *Hydrometallurgy*, **191**, 105184.

Bai G., Teng W., Wang X., Qin J., Xu P. & Li P. (2010) Alkali desilicated coal fly ash as substitute of bauxite in lime-soda sintering process for aluminum production. *Transactions of Nonferrous Metals Society of China*, **20**, 169–175.

Battaglia S. (2004) Variations in the chemical composition of illite from five geothermal fields: a possible geothermometer. *Clay Minerals*, **39**, 501–510.

Bazhirov T.S., Dauletiyarov M.S., Bazhirov N.S., Serikbayev B.E. & Bazhirova K.N. (2020) Physical and chemical studies of slag of production of low-carbon ferrochrome – component of heat-resistant binder material. *Izvestiya Vysshikh Uchebnykh Zavedeniy Khimiya Khimicheskaya Tekhnologiya*, **63**, 58–64.

Biagioni C. & Pasero M. (2014) The systematics of the spinel-type minerals: an overview. *American Mineralogist*, **99**, 1254–1264.

Birinci M., Uysal T., Erdemoğlu M., Porgalı E. & Barry T. (2017) Acidic leaching of thermally activated pyrophyllite ore from Puturge (Malatya–Turkey) deposit. Presented at: *XVII Balkan Mineral Processing Congress*, 1–3 November, Antalya, Turkey.

Brichkin V.N., Kurtenkov R.V., ElDeeb A.B. & Bormotov I.S. (2019) State and development options for the raw material base of aluminum in non-bauxite regions. *Obogashchenie Rud*, **4**, 31–37.

Cao Z., Cao Y.D., Dong H.J., Zhang J.S. & Sun C.B. (2016) Effect of calcination condition on the microstructure and pozzolanic activity of calcined coal gangue. *International Journal of Mineral Processing*. **146**, 23–28.

Chalouati Y., Bennour A., Mannai F., & Srasra E. (2020) Characterization, thermal behaviour and firing properties of clay materials from Cap Bon Basin, north-east Tunisia, for ceramic applications. *Clay Minerals*, **55**, 351–365.

Chou K.S. & Burnet G. (1981) Formation of calcium aluminates in the lime-sinter process. *Cement and Concrete Research*, **11**, 167–174.

D'Elia A., Pinto D., Eramo G., Giannossa L., Ventruti G. & Laviano R. (2018) Effects of processing on the mineralogy and solubility of carbonate-rich clays for alkaline activation purpose: mechanical, thermal activation in red/ox atmosphere and their combination. *Applied Clay Science*, **152**, 9–21.

Drits V., Sakharov B., Dorzhieva O., Zviagina B. & Lindgreen H. (2019) Determination of the phase composition of partially dehydroxylated kaolinites by modelling their X-ray diffraction patterns. *Clay Minerals*, **54**, 309–322.

Dubovikov O.A., Brichkin V.N., Ris A.D. & Sundurov A.V. (2018) Thermochemical activation of hydrated aluminosilicates and its importance for alumina production. *Non-ferrous Metals*, **2**, 3–15.

ElDeeb A.B.S. & Brichkin V.N. (2018) Egyptian aluminum containing ores and prospects for their use in the production of aluminum. *International Journal of Scientific Engineering and Research*, **9**, 721–731.

ElDeeb A.B., Brichkin V.N., Kurtenkov R.V. & Bormotov I.S. (2019) Extraction of alumina from kaolin by a combination of pyro- and hydrometallurgical processes. *Applied Clay Science*, **172**, 146–154.

ElDeeb A.B., Brichkin V.N., Bertau M., Savinova Yu.A. & Kurtenkov R.V. (2020a) Solid state and phase transformation mechanism of kaolin sintered with limestone for alumina extraction. *Applied Clay Science*, **196**, 105771.

ElDeeb A.B., Brichkin V.N., Povarov V.G. & Kurtenkov R.V. (2020b) The activating effect of carbon during sintering the limestone–kaolin mixture. *Tsvetnye Metally*, **7**, 18–25.

ElDeeb A.B., Brichkin V.N., Sizyakov V.M. & Kurtenkov R.V. (2020c) Effect of sintering temperature on the alumina extraction from kaolin. Pp. 136–145 in: *Advances in Raw Material Industries for Sustainable Development Goals* (E. Litvinenko, editor). CRC Press, Boca Raton, FL, USA.

ElDeeb A.B., Brichkin V.N., Kurtenkov R.V. & Bormotov I.S. (2021) Study of the peculiarities of the leaching process for self-crumbling limestone–kaolin cakes. *Obogashchenie Rud*, **2021**, 27–32.

Erdemoğlu M. & Baláž P. (2012) An overview of surface analysis techniques for characterization of mechanically activated minerals. *Miner Processing and Extractive Metallurgy Review*, **33**, 65–88.

Erdemoğlu M., Birinci M. & Uysal T. (2018) Alumina production from clay minerals: current reviews. *Journal of Polytechnic*, **21**, 387–396.

Gao Y., Liang K., Gou Y., Wei S., Shen W. & Cheng F. (2020) Aluminum extraction technologies from high aluminum fly ash. *Reviews in Chemical Engineering*, **37**, 885–906.

Gasparini E., Tarantino S.C., Ghigna P., Riccardi M.P., Cedillo-González E.I., Siligardi C. & Zema M. (2013) Thermal dehydroxylation of kaolinite under isothermal conditions. *Applied Clay Science*, **80**, 417–425.

Guo Y., Yan K., Cui L., Cheng F. & Lou H.H. (2014) Effect of Na_2CO_3 additive on the activation of coal gangue for alumina extraction. *International Journal of Mineral Processing*, **131**, 51–57.

Guo Y., Yan K., Cui L. & Cheng F. (2016) Improved extraction of alumina from coal gangue by surface mechanically grinding modification. *Powder Technology*, **302**, 33–41.

Húlan T., Štubňa I., Shishkin A., Ozolins J., Csáki, Š, Bačík P. & Fridrichová J. (2019) Development of Young's modulus of natural illitic clay during the heating and cooling stages of firing. *Clay Minerals*, **54**, 229–233.

Ivanov M.A., Pak V.I., Nalivayko A.Yu., Kirov S.S. & Bozhko G.G. (2019) Prospects of using Russian high silicon raw materials in alumina production. *Bulletin of the Tomsk Polytechnic University. Geo Assets Engineering*, **330**, 93–102.

Jadhav R. & Debnath N.C. (2011) Computation of X-ray powder diffractograms of cement components and its application to phase analysis and hydration performance of OPC cement. *Bulletin of Materials Science*, **34**, 1137–1150.

Karbalaei Saleh D., Abdollahi H., Noaparast M. & Fallah Nosratabad A. (2019). Dissolution of aluminium from metakaolin with oxalic, citric and lactic acids. *Clay Minerals*, **54**, 209–217.

Kaußen F.M. & Friedrich B. (2018) Phase characterization and thermochemical simulation of (landfilled) bauxite residue ('red mu') in different alkaline processes optimized for aluminum recovery. *Hydrometallurgy*, **176**, 49–61.

Küster D., Kaufhold S., Limam E., Jatlaoui O., Ba O., Mohamed A. *et al.* (2021) Investigation of unexplored kaolin occurrences in southern Mauritania and preliminary assessment of possible applications. *Clay Minerals*, **56**, 126–139.

Li G., Zeng J., Luo J., Liu M., Jiang T. & Qiu G. (2014a) Thermal transformation of pyrophyllite and alkali dissolution behavior of silicon. *Applied Clay Science*, **99**, 282–288.

Li H., Hui J., Wang C., Bao W. & Sun Z. (2014b) Extraction of alumina from coal fly ash by mixed-alkaline hydrothermal method. *Hydrometallurgy*, **147–148**, 183–187.

Li X., Wang H., Zhou Q., Qi T., Liu G. & Peng Z. (2019) Efficient separation of silica and alumina in simulated CFB slag by reduction roasting-alkaline leaching process. *Waste Management*, **87**, 798–804.

Li P., Li J., Chen Z., Liu X., Huang Z. & Zhou F. (2021) Compositional evolution of the muscovite of Renli pegmatite-type rare-metal deposit, northeast Hunan, China: implications for its petrogenesis and mineralization potential. *Ore Geology Reviews*, **138**, 104380.

Liew Y.M., Kamarudin H., Mustafa Al Bakri A.M., Luqman M., Khairul Nizar I., Ruzaidi C.M. & Heah C.Y. (2012) Processing and characterization of calcined kaolin cement powder. *Construction and Building Materials*, **30**, 794–802.

Mejía De Gutiérrez R., Torres J., Vizcayno C. & Castello R. (2008) Influence of the calcination temperature of kaolin on the mechanical properties of mortars and concretes containing metakaolin. *Clay Minerals*, **43**, 177–183.

https://doi.org/10.1180/clm.2022.7 Published online by Cambridge University Press

Mikhailova Yu.A., Konopleva N.G., Yakovenchuk V.N., Ivanyuk G.Yu., Menshikov Yu.P. & Pakhomovsky Ya.A. (2007) Corundum-group minerals in rocks of the Khibiny alkaline pluton, Kola Peninsula. *Geology of Ore Deposits*, **49**, 41–54.

Murray H.H. (2006) Structure and composition of the clay minerals and their physical and chemical properties. *Developments in Clay Science*, **2**, 7–31.

Nzeukou Nzeugang A., Ouahabi M., Aziwo B., Mache J., Mefire Mounton H. & Fagel N. (2018) Characterization of kaolin from Mankon, northwest Cameroon. *Clay Minerals*, **53**, 563–577.

Olaremu A.G. (2015) Sequential leaching for the production of alumina from a Nigerian clay. *International Journal of Engineering Technology, Management and Applied Sciences*, **3**, 103–109.

Pak V.I., Kirov S.S., Nalivaiko A.Y., Ozherelkov D.Y. & Gromov A.A. (2019) Obtaining alumina from kaolin clay *via* aluminum chloride. *Materials*, **12**, 1–12.

Pontikes Y., Jones P.T., Geysen D. & Blanpain B. (2010) Options to prevent dicalcium silicate-driven disintegration of stainless-steel slags. *Archives of Metallurgy and Materials*, **55**, 1167–1172.

Ptáček P., Opravil T., Šoukal F., Havlica J. & Holešinský R. (2013) Kinetics and mechanism of formation of gehlenite, Al–Si spinel and anorthite from the mixture of kaolinite and calcite. *Solid State Science*, **26**, 53–58.

Qiao X.C., Si P. & Yu J.G.A. (2008) A systematic investigation into the extraction of aluminum from coal spoil through kaolinite. *Environmental Science and Technology*, **42**, 8541–8546.

Qiu G.Z., Jiang T., Li G.H., Fan X.H. & Huang Z.C. (2004) Activation and removal of silicon in kaolinite by thermochemical process. *Scandinavian Journal of Metallurgy*, **33**, 121–128.

Scorzelli R., Bertolino L., Luz A., Duttine M., Silva F. & Munayco P. (2008) Spectroscopic studies of kaolin from different Brazilian regions. *Clay Minerals*, **43**, 129–135.

Sizyakov V.M. (2016) Chemical and technological mechanisms of an alkaline aluminum silicates sintering and a hydrochemical sinter processing. *Journal of Mining Institute*, **217**, 102–112.

Sizyakov V.M. & Brichkin V.N. (2018) About the role of hydrafed calcium carboaluminates in improving the technology of complex processing of nephelines. *Journal of Mining Institute*, **231**, 292–298.

Sizyakov V.M., Dubovikov O.A. & Nikolaeva N.V. (2013a) The role of calcium oxide in the thermochemical conditioning of bauxite. *Journal of Mining Institute*, **202**, 14–19.

Sizyakov V.M., Dubovikov O.A., Nikolaeva N.V. & Kalashnikova M.I. (2013b) The role of mineralized additives in the alumina phase transformation process. *Journal of Mining Institute*, **202**, 48–55.

Sizyakov V.M., Bazhin V.Yu. & Sizyakova E.V. (2016) Feasibility study of the use of nepheline-limestone charges instead of bauxite. *Metallurgist*, **59**, 1135–1141.

Smith P. (2009) The processing of high silica bauxites – review of existing and potential processes. *Hydrometallurgy*, **98**, 162–176.

Stange K., Lenting C. & Geisler T. (2017) Insights into the evolution of carbonate-bearing kaolin during sintering revealed by *in situ* hyperspectral Raman imaging. *Journal of the American Ceramic Society*, **101**, 1–14.

Sule R. & Sigalas I. (2020) Influence of excess alumina on mullite synthesized from pyrophyllite by spark plasma sintering. *Clay Minerals*, **55**, 166–171.

Tang A., Su L., Li C. & Wei W. (2010) Effect of mechanical activation on acid-leaching of kaolin residue. *Applied Clay Science*, **48**, 296–299.

Tantawy M.A. & Alomari A.A. (2019) Extraction of alumina from Nawan kaolin by acid leaching. *Oriental Journal of Chemistry*, **35**, 1013–1021.

Tian Y., Pan X., Yu H., Han Y., Tu G. & Bi S. (2016a) An improved lime sinter process to produce Al_2O_3 from low-grade Al-containing resources. Pp. 5–9 in: *Light Metals 2016* (E. Williams, editor). Springer, Berlin, Germany.

Tian Y., Pan X., Yu H. & Tu G. (2016b) Formation mechanism of calcium aluminate compounds based on high-temperature solid-state reaction. *Journal of Alloys and Compounds*, **670**, 96–104.

Toama H.Z., Al-Ajeel A.A. & Jumaah A.H. (2018) Studying the efficiency of lime-soda Sinter process to extract alumina from colored kaolinite ores using factorial technique of design of experiments. *Engineering and Technology Journal*, **36**, 500–508.

Uddin F. (2008) Clays, Nano clays, and montmorillonite minerals. *Metallurgical and Materials Transactions A*, **39**, 2804–2814.

Valeev D., Pak V., Mikhailova A., Gol'Dberg M., Zheleznyi M., Dorofievich I. *et al.* (2016) Extraction of aluminium by autoclave hydrochloric acid leaching of boehmite–kaolinite bauxite. Pp. 23–28 in: *Light Metals 2016* (E. Williams, editor). Springer, Berlin, Germany.

Vdovets A.Z. (2020) Variability of alunite quartzite composition as a reflection of the characteristics of its genesis. *Geology of Ore Deposits*, **62**, 138–162.

Wang B., Sun H., Guo D. & Zhang X. (2011) Effect of Na_2O on alumina leaching property and phase transformation of MgO-containing calcium aluminate slags. *Transactions of Nonferrous Metals Society, China*, **21**, 2752–2757.

Wang B., Chu W., Hao Y., Rong S. & Sun H. (2017) Synthesis and alumina leaching mechanism of calcium sulphoaluminate. *Transactions of Nonferrous Metals Society, China*, **27**, 2090–2095.

Xu X.H., Lao X.B., Wu J.F., Zhang Y.X., Xu X.Y. & Li K. (2015) Microstructural evolution, phase transformation, and variations in physical properties of coal series kaolin powder compact during firing. *Applied Clay Science*, **115**, 76–86.

Yan K., Guo Y., Fang Li, Cui Li, Cheng F. & Li T. (2017) Decomposition and phase transformation mechanism of kaolinite calcined with sodium carbonate. *Applied Clay Science*, **147**, 90–96.

Yu H., Pan X., Wang B., Zhang W., Sun H. & Bi S. (2012) Effect of Na_2O on the formation of calcium aluminates in the $CaO–Al_2O_3–SiO_2$ system. *Transactions of Nonferrous Metals Society, China*, **22**, 3108–3112.

Yu H., Pan X., Liu B., Wang B. & Bi S. (2014) Effect of iron oxides on the activity of calcium aluminate clinker in $CaO–Al_2O_3–SiO_2$ system. *Journal of Iron and Steel Research International*, **21**, 990–994.

Yu H., Pan X., Dong K. & Wu Y. (2019) Effect of P addition on mineral transition of $CaO–Al_2O_3–SiO_2$ system during high-temperature sintering. *Transactions of Nonferrous Metals Society, China*, **29**, 650–656.

Yuan S., Han Y., Li Y., Gao P. & Yu J. (2018) Effect of calcination temperature on activation behaviors of coal-series kaolin by fluidized bed calcination. *Physicochemical Problems and Mineral Processing*, **54**, 590–600.

Zhang S., Ou X., Qiang Y., Niu J. & Komarneni S. (2015a) Thermal decomposition behavior and de-intercalation mechanism of acetamide intercalated into kaolinite by thermoanalytical techniques. *Applied Clay Science*, **114**, 309–314.

Zhang D., Pan X., Yu H. & Zhai Y. (2015b) Mineral transition of calcium aluminate clinker during high-temperature sintering with low-lime dosage. *Journal of Material Science and Technology*, **31**, 1244–1250.

Zhou C.C., Liu G.J., Yan Z.C., Fang T. & Wang R.W. (2012) Transformation behavior of mineral composition and trace elements during coal gangue combustion. *Fuel*, **97**, 644–650.

Zhou C.C., Liu G.J., Fang T. & Lam P.K.S. (2015) Investigation on thermal and trace element characteristics during co-combustion biomass with coal gangue. *Bioresource Technology*, **175**, 454–462.

https://doi.org/10.1180/clm.2022.7 Published online by Cambridge University Press